Hindawi
International Journal of Aerospace Engineering
Volume 2022, Article ID 3471421, 10 pages
https://doi.org/10.1155/2022/3471421

Research Article

Effect of Cooling Header on the Hydrocarbon Fuel Flow Distribution in a Regenerative Cooling Channel

Liang Yin,[1] **Jiaqiang E**,[2] **and Jie Ding**[1]

[1]*College of Mechanical Engineering, Hunan University of Arts and Science, Changde 415000, China*
[2]*College of Mechanical and Vehicle Engineering, Hunan University, Changsha, Hunan 410073, China*

Correspondence should be addressed to Liang Yin; yl88222@126.com

Received 23 May 2022; Revised 4 July 2022; Accepted 11 August 2022; Published 8 September 2022

Academic Editor: Jun-Wei Li

Regenerative cooling technology is the most widely used cooling technology in liquid rocket engines, and flow distribution is very important for regenerative cooling heat transfer. In this work, the flow distribution characteristics of *Z*-type parallel channels were studied through numerical simulation, and the effects of flow area ratio, inlet header shape, and inlet aspect ratio were analyzed. Results showed that changing the inlet cooling header can improve the uniform distribution of flow rate effectively. The nonuniformity coefficient and fuel temperature varied with change in the flow area ratio, inlet header shape, and inlet aspect ratio. The maximum temperature of the wall decreased from 1334.52 K to 1220.61 K when the flow area ratio was changed from 1 to 0.25. An appropriate decrement in the inlet header shape was beneficial to the uniform flow distribution. The inlet aspect ratio should be reduced properly to ensure that each channel experiences similar pressure drop. This research has a certain reference value for the structural design of regenerative cooling channels.

1. Introduction

Regenerative cooling technology is the most widely used cooling technology in liquid rocket engines [1–3]. During regenerative cooling, the coolant enters the cooling channel at a low temperature (usually lower than the critical temperature) under supercritical pressure. After heat is absorbed from the combustion chamber, the fuel temperature gradually increases and finally reaches the supercritical state. The process of fluid flow and heat transfer in the regenerative cooling channels of liquid rocket engines is very complex. In particular, fluid density [4], viscosity, specific heat, and the thermal diffusion coefficient change dramatically [5, 6] near the quasicritical point. The buoyancy and flow acceleration caused by the change in physical parameters have a massive effect on the heat transfer of the fluid [7–9]. Under high temperatures, coking and carbon deposition caused by the pyrolysis of hydrocarbon fuel can also cause the blockage of regenerative cooling channels [10–15]. The application of the heat released from combustion and aerodynamic heating to the wall surface with unsteady and uneven thermal loads [16–18] results in uneven cooling flow distribution. The uneven flow distribution is one of the direct reasons for the uneven temperature distribution. This will eventually cause excessive flow deviation, temperature deviation between channels, as well as the unreasonable utilization of fuel cooling capacity and waste of finite heat sink.

Only a few studies have been conducted on inlet header shape-related flow distribution in regenerative cooling channels with hydrocarbon fuel as the working medium. Ran [19] studied the flow distribution characteristics of aviation kerosene RP-3 in vertical parallel *U*-pipes under supercritical pressure and analyzed the effects of working medium temperature, system pressure, and heat flux density on flow distribution characteristics. Their study showed that uneven heat flux had a significant effect on flow distribution. Flow distribution in each branch pipe was uneven when kerosene reached the quasicritical point. Increasing

the system pressure can effectively suppress the unbalance of flow distribution in each branch of parallel pipes and enhance system stability. Feng [20] took the coupling effect of the flow and cracking processes of supercritical hydrocarbon fuel in pipelines as the research object and established one-dimensional and two-dimensional calculation models for the coupling of the flow cracking of supercritical hydrocarbon fuel. The effects of the coupling effect of flow cracking on the heat sink of fuel, heat, and mass transfer mechanism of the chemical reaction flow field and flow field optimization of local special cooling structures in cooling channels were studied. Jing [21] proposed several different nonuniform regenerative cooling channel structures and used numerical simulation to analyze the influence of inlet and outlet structures and relative inlet and outlet widths on flow and heat transfer characteristics in channels. Their results demonstrated that when $\Omega = 1$, violent nonuniform flow exists in the channel near the inlet pipe, and the flow distribution is more sensitive to the inlet position than to the outlet position. Tao [22] established a two-dimensional numerical model of the pyrolysis of *n*-decane under supercritical conditions and studied the effects of pyrolysis on the heat transfer characteristics and flow resistance of *n* -decane. Jiang [23] investigated the influences of the header geometry on hydrocarbon fuel flow distribution in compact parallel channels. The classical *U*-type configuration was adopted for the parallel system.

Changing the distribution of thermal loads and the variation of channel sections is a simple and effective design idea for improving uneven flow distribution. Specifically, a cooling effect can be obtained by changing the size parameters of passages (wall thickness, rib width, length-to-width ratio of the passage, and flow area) or increasing the coolant flow rate. In this work, the regenerative cooling channel model of liquid rocket engines is simplified, and the typical *Z*-type structure is used for simulation analysis. The influence of the structural parameters of inlet header of regenerative cooling channel on flow distribution and cooling effect under even heat flux is numerically simulated via the fluid–solid/thermal coupling analysis method.

2. Model

2.1. Problem Description. For the analysis in this work, the calculation domain of regenerative cooling adopts a typical *Z*-type structure with the total width of 36.4 mm and the channel length of 300 mm. A total of seven parallel channels M1–M7 with the inlet and outlet areas of 25–75 mm^2 are used as shown in Figure 1. The values of the geometric parameters used in the simulation are shown in Table 1. Under all the variations in parameters conducted in this study, the outlet header dimensions and shape change as well as the inlet header.

The effect of thermal coupling on flow distribution under the rib is considered. The working process of the regenerative cooling channel of liquid rocket engines is more severe and complex than the hypersonic vehicle. For example, it presents higher heat flux, larger fuel flow, and more drastic physical property changes. This work mainly focuses on the features of the nonpyrolysis zone. The following assumptions are adopted:

(1) The influence of fuel cracking and coking is not considered

(2) The effect of fuel phase transition during flow is not considered

(3) The influence of thermal load on regeneration channel deformation is not considered

(4) The influence of unsteady and heterogeneous thermal loads is not considered

2.2. Numerical Method. The continuity, momentum, and energy equations for the fluid region are listed as follows:

$$\nabla \cdot \left(\rho \vec{u}\right) = 0, \tag{1}$$

$$\nabla \cdot \left(\rho \vec{u}\,\vec{u}\right) = -\nabla p + \nabla \cdot \tau_{eff}, \tag{2}$$

$$\nabla \cdot \left(\rho \vec{u} e_t\right) = -\nabla \cdot \left(\lambda_{eff} \nabla T\right) - \nabla \cdot \left(\rho \vec{u}\right). \tag{3}$$

In Equation (3), considering that the flow velocity (relative to local sound speed, about 1500 m/s) in this paper is relatively low, the terms related to viscous dissipation are ignored. The buoyancy effect can be determined by the formula [21] $\mathrm{Bo} = \mathrm{Gr}/\mathrm{Re}^{3.425}\mathrm{Pr}^{0.8}$. When Bo is less than 5.6×10^{-7}, it can be ignored. In this work, the buoyancy effect is not considered.

In the solid domain, the thermal conduction equation is numerically solved.

$$\nabla \cdot (\lambda \nabla T) = 0. \tag{4}$$

The commercial software Fluent 19.2 was used for simulation calculation. The Reynolds number can be calculated by the formula $\mathrm{Re} = ul/\nu$. Considering the low-speed flow problem under high heat flux condition, the Realizable $k-\varepsilon$ turbulence model was selected for calculation. The SIMPLEC algorithm and second order upwind discretization were used in the simulation process. In these works, the wall grid of the main area is guaranteed to be $y^+ < 1.0$, the corresponding height of the first layer grid is set to 0.002 mm, and the grid is arranged in a gradient of 1.15.

The mass flow inlet condition is adopted. The mass flow rate is calculated from the heat flux, and the total mass flow of coolant is 202 g/s. In order to ensure that the hydrocarbon fuel in the channel is in the nonpyrolysis zone, the outlet pressure is set to be 0.45 MPa. The wall thickness δ is 1.2 mm.

T_{wg} is the surface temperature of the gas side wall, and the limit temperature that GH3128 can withstand is approximately 1400 K. T_{wc} is the side wall temperature of the coolant. The heat flux is set as 4.38 MW/m^2 to ensure that the fuel is mostly in the nonpyrolysis zone. In this study, the heat flux 4.38 MW/m^2 is a given value, which is obtained from the actual engine heat flux [23]. The other wall is set

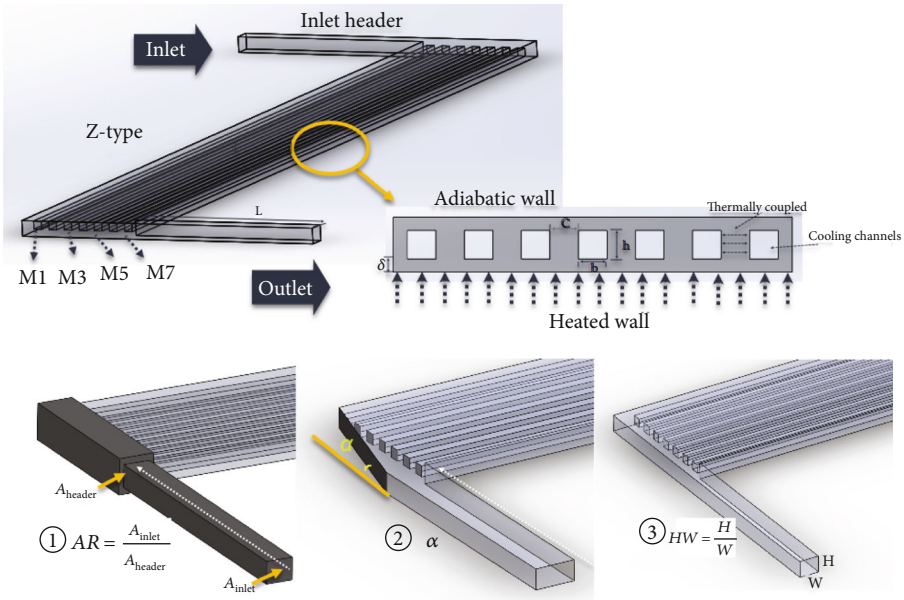

Figure 1: The schematic of regenerative cooling channel.

Table 1: Values of the geometric used in the simulation.

Parameter	Description	Value
c	Spacing of channel	2.6 mm
h	Height of channel	2.6 mm
b	Width of channel	2.6 mm
δ	Thickness of the wall	1.2 mm
L	Length of inlet/outlet header	63.6 mm

as an adiabatic nonslip wall boundary. The coupled boundary condition is adopted at the fluid-solid interface region. The mathematical form is given in Equation (5).

$$h_c(T_{wc} - T_\infty) = -\lambda\left(\frac{dT}{dn}\right)_w, \quad (5)$$

where T_∞ is the temperature of coolant, h_c is the heat transfer coefficient.

Kerosene is selected as the coolant. The physical parameters change drastically when the temperature of kerosene exceeds the critical temperature. Density, dynamic viscosity, and thermal conductivity decrease with the increase in temperature. In this work, the physical parameters are given as piecewise functions [24].

The density of kerosene varies with temperature, and it is given in

$$\rho(T) = \begin{cases} 1003 - 0.76T, 293 < T < 613K \\ 2596 - 3.36T, 613 < T < 723K \\ 446 - 0.386T, 723 < T < 1000K \end{cases} \left(\text{kg/m}^3\right). \quad (6)$$

The specific heat of kerosene varies with temperature, and it is given in

$$c_p(T) = \begin{cases} 0.167 - 0.0001T, 293 < T < 613K \\ 0.4448 - 0.0007T, 613 < T < 740K \\ -0.1 + 0.00017T, 740 < T < 1000K \end{cases} (\text{J/kg} \cdot \text{K}). \quad (7)$$

The heat conductivity coefficient of kerosene varies with temperature, and it is given in Equation (8)

$$\lambda(T) = \begin{cases} 0.697 + 0.004T, 293 < T < 613K \\ -32.079 + 0.0536T, 613 < T < 740K \\ 65.66 - 0.1368T + 7.148 \times 10^{-5}T^2, 740 < T < 1000K \end{cases} (\text{W/m} \cdot \text{K}). \quad (8)$$

The material of the solid is high-temperature alloy GH3128. The density of GH3128 is 8810 kg/m^3, and the specific heat is 394 J/kg·K. The thermal conductivity coefficient is given by the following fitting polynomial [25]:

$$\lambda = 6.765 + 0.01155T\text{-}1.944 \times 10^{-6}T^2 (\text{W/m} \cdot \text{K}). \quad (9)$$

The solutions were considered as converging when the residuals reach the minimum values after falling for more than two orders of magnitude, and the differences of outlet fuel temperature of all branch channels is less than 0.1 K in continuous iterations. In all cases, the differences of inlet and outlet mass flow rate of all channels are less than 1×10^{-5} kg/s.

2.3. Analysis Parameters. Relative standard deviation (RSD) is used to characterize the rationality of mass flow rate

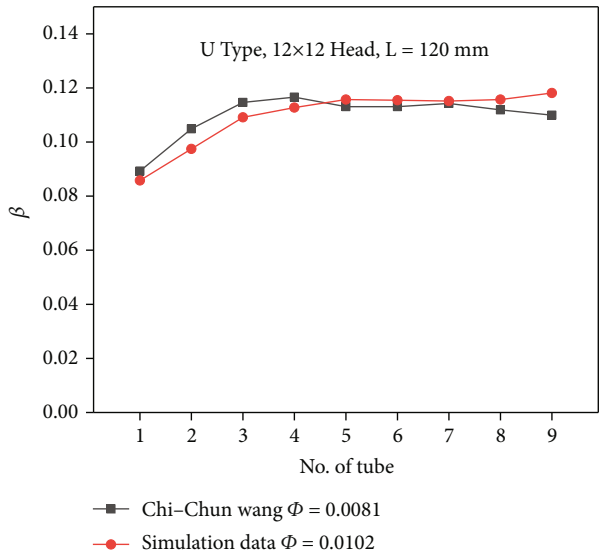

Figure 2: Verification of numerical methods.

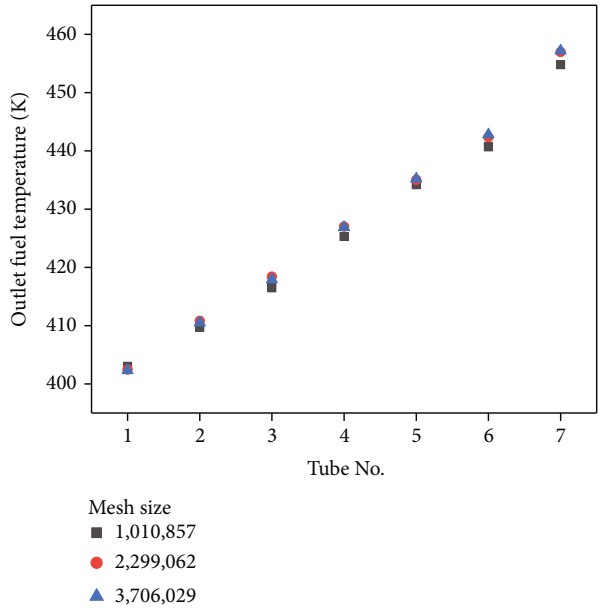

Figure 3: Grid independence study.

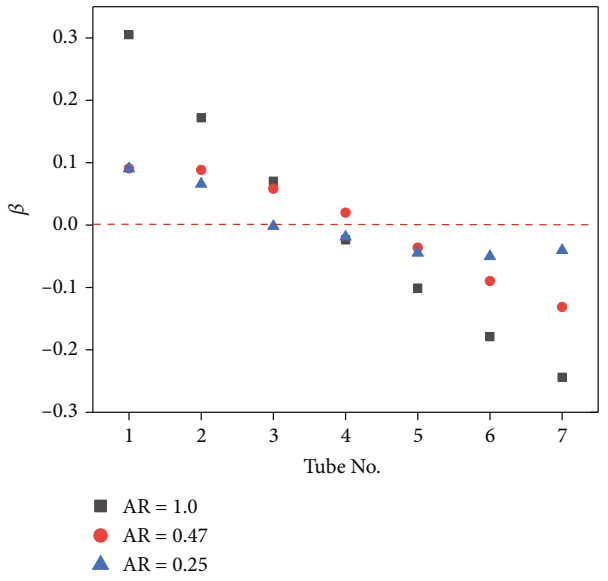

Figure 4: Nonuniformity coefficient with different AR values.

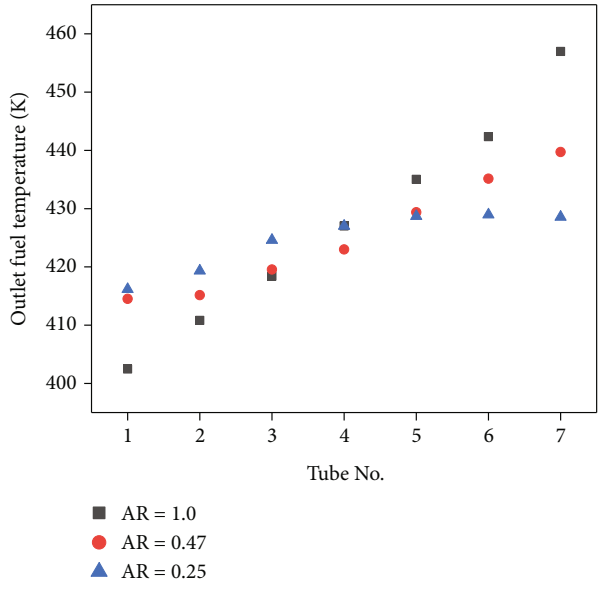

Figure 5: Outlet fuel temperature with different AR values.

distribution. Under the condition of uniform heat flux, a small RSD is indicative of the highly uniform distribution of mass flow rate. The deviation of mass flow rate distribution is defined as

$$\Phi_m = \sqrt{\frac{1}{n}\sum_{i=1}^{n}\beta_i^2}, \tag{10}$$

where n is the number of the channels.

β_i is the nonuniformity coefficient of each channel:

$$\beta_i = \frac{m_i - \bar{m}}{\bar{m}}, \tag{11}$$

where m_i is the mass flow rate of channel i and $\bar{m}$ is the average mass flow rate of all the channels. The mass flow is calculated at the exit. The value of $\bar{m}$ and outlet fuel temperature T_{out} is calculated from surface integrals, $(1/A)\int \phi dA = (1/A)\sum_{i=1}^{n}\phi_i|A_i|$.

2.4. Model Validation. The turbulence model adopted for the microparallel channels and the coupled heat transfer between the channels must be considered to verify the accuracy of the numerical modeling of flow distribution in parallel channels. A comparative study of various turbulence models is made in the literature [26], and it is found that there is little difference between the SST k -ε turbulence model and the Realizable k -ε turbulence model. In this

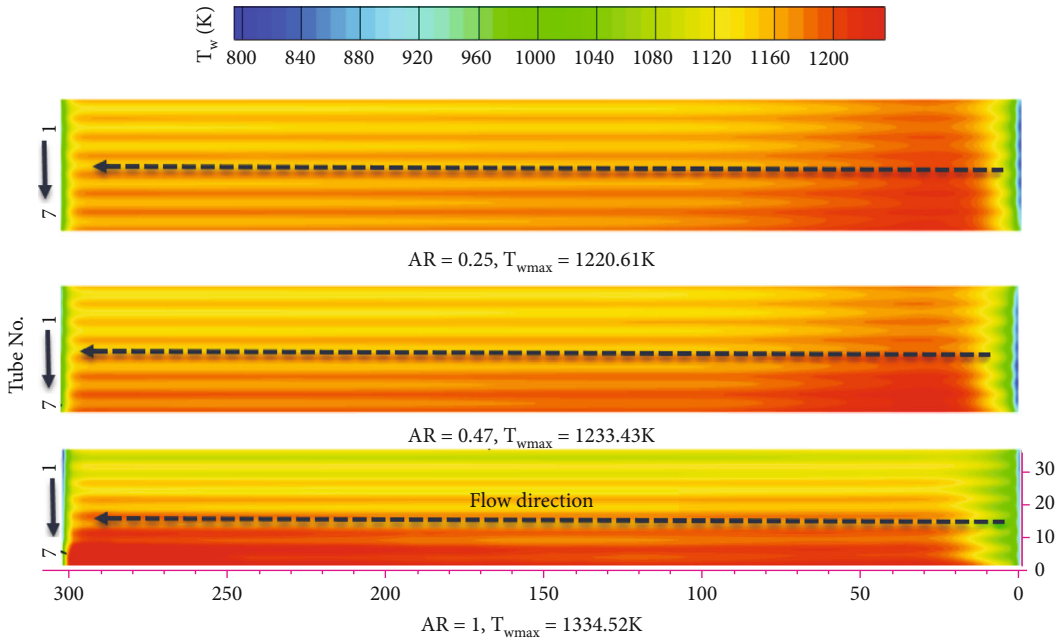

Figure 6: The wall temperature contours with different AR values.

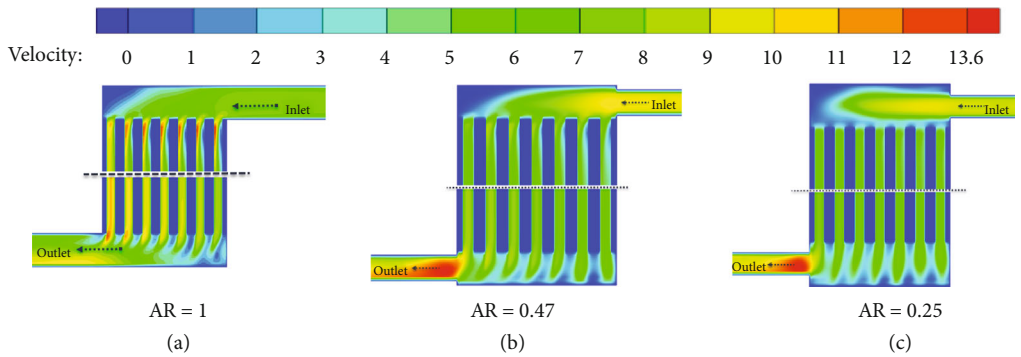

Figure 7: The velocity fields in the center planes with different AR values: (a) AR = 1, (b) AR = 0.47, and (c) AR = 0.25.

work, the experimental results of Wang et al. [26] are compared with the simulation results for analysis and verification. A *U*-type structure is selected for comparative analysis. The inlet header has the dimensions of 12 mm × 12 mm and the total length of 120 mm. Figure 2 presents the comparison between the numerical simulation results and the literature. The results show that the Realizable k -ε turbulence model selected in this work and the fluid–solid thermal coupling model can effectively predict the flow distribution in the parallel channel. The maximum error is approximately 6.92%.

2.5. Grid Convergence Analysis. Fine mesh size can be beneficial for obtaining computational accuracy and good spatial resolution in simulations. In this study, three different hexahedral meshes, namely, 101 0857, 229 9062, and 370 6029, are adopted for the computational domain to ensure grid independence. The influence on outlet fuel temperature is analyzed under the same conditions shown in Figure 3. The outlet fuel temperatures between the 229 9062 and 370 6029 meshes are nearly the same in the parallel channels, indicating that the solution is mesh converged. Therefore, 229 9062 grids are selected for this simulation.

3. Results and Discussions

3.1. Effects of Flow Area Ratio. The flow area ratio of the inlet and the inlet header, which is represented by the AR value, is an important design parameter of parallel channels. The AR value is defined as the formula given below. During the comparison, the area of the inlet is kept constant, and the area of inlet header is 30, 64,144 mm^2.

$$AR = \frac{A_{inlet}}{A_{header}}, A_{inlet} = const = 30mm^2. \quad (12)$$

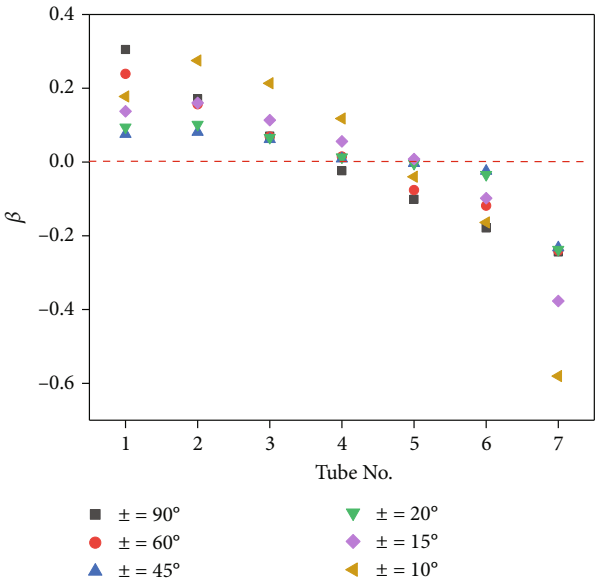

Figure 8: Nonuniformity coefficient with different α values.

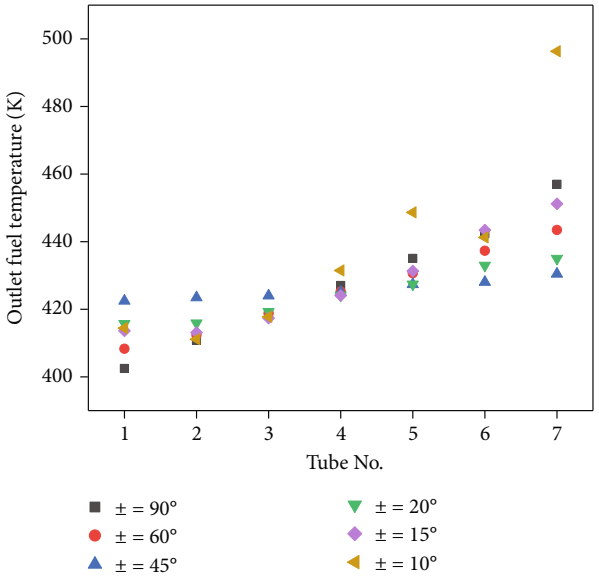

Figure 9: Outlet fuel temperature with different α values.

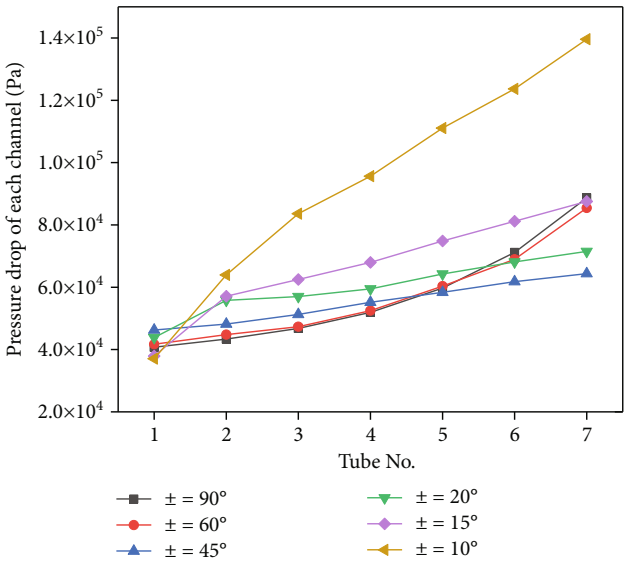

Figure 10: The pressure drop of each channel with different α values.

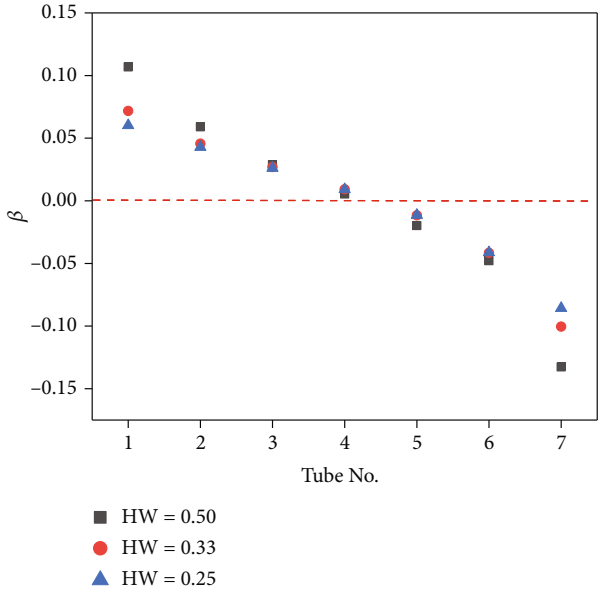

Figure 11: Nonuniformity coefficient with different HW values.

The inlet header decreases with the AR value increases. As inlet header increases, the velocity decreases, and the more evenly the flow is distributed. As shown in Figure 4, the nonuniformity coefficient shows great differences with the change in AR. It decreases when AR declines. Therefore, flow uniformity can be effectively improved by increasing the area of the inlet header. Figure 5 shows that when AR = 0.25, the outlet fuel temperature in each channel shows little changes. Tube No. 1 exhibits the highest mass flow rate because it has the lowest pressure drop.

The cooling effect as a function of different AR values is shown in Figure 6. The maximum wall temperature increases with the decrease in the AR value. The maximum temperature of the wall decreases from 1334.52 K to 1220.61 K, and the overall temperature distribution shows increased uniformity. The outlet wall temperature can also be seen to greatly differ due to the different flow rates of each channel. This situation indicates that the AR value is a very effective design factor for the optimization of flow distribution and cooling.

The flow area ratio affects the flow area of the inlet and the inlet header. The velocity distribution along the main flow direction of the inlet and inlet header decides the velocity distribution of each channel. The channel cross-section

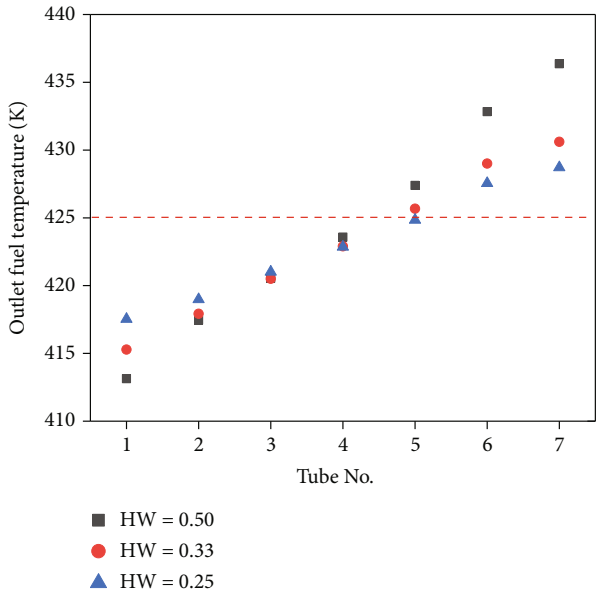

Figure 12: Outlet fuel temperature with different HW values.

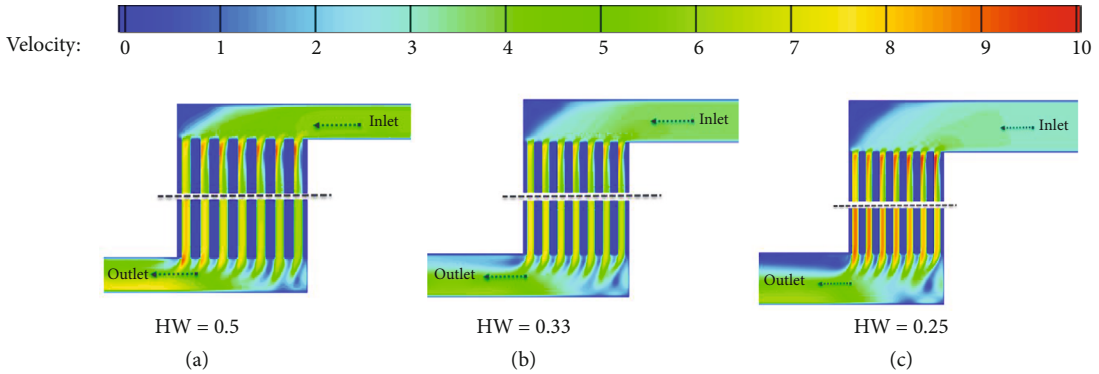

Figure 13: The velocity fields in the center planes with different HW values: (a) HW = 0.5, (b) HW = 0.33, and (c) HW = 0.25.

decreases with the increase of flow area ratio. The velocity fields in the center planes with different AR values is shown in Figure 7. It can be seen that the velocity in the inlet when AR = 0.25 is obvious higher than those of other AR values. The change of flow area leads to the decrease of inlet header velocity, which is beneficial to the uniform flow distribution.

3.2. Effects of Inlet Header Shape. Geometrical structure and operating conditions are the most direct factors affecting flow distribution in parallel channels. The change in geometric structure leads to changes in the hydraulic diameter of each channel, and the change in fluid velocity and flow resistance affects flow distribution. The influence of inlet header shape α on flow distribution is studied.

Figure 8 shows the nonuniformity coefficients of each channel with a different inlet header shape α, where $\alpha = 90^{\circ}$ is a rectangular confluence structure. As the inlet header shape α is decreased, the nonuniformity coefficients of each channel decrease first and then increase. When α is 60° and 90°, the nonuniformity coefficients show little differences. The mass flow rate of channel No. 7 is the lowest, and the outlet fuel temperature is the highest, as shown in Figure 9. The flow distribution in each channel mainly depends on the pressure drop, and the change in pressure drop can be attributed to the thermal load deviation and the geometric structure as illustrated in Figure 10. It can be seen that the pressure drop of each channel changes little when $\alpha = 45^{\circ}$. The change of pressure drop is proportional to the change of flow rate in each channel. Therefore, under the same mass flow rate and thermal load condition, the flow area decreases and the flow velocity increases with the decrease in the inlet header shape α. The mass flow rate in each channel also increases to match the equilibrium relationship of the inlet and outlet pressure drop. Therefore, appropriately decreasing the inlet header shape α is beneficial to uniform flow distribution.

3.3. Effects of Inlet Aspect Ratio. Inlet aspect ratio is another important parameter affecting flow distribution. The aspect ratio of the inlet is defined as follows:

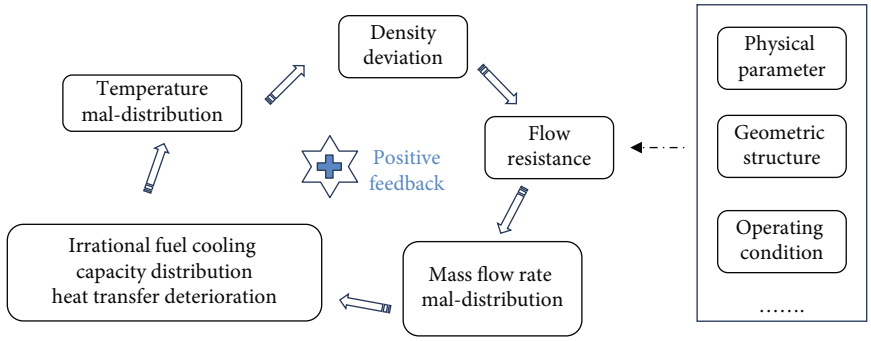

Figure 14: Influence mechanism of flow distribution in parallel channels.

$$\mathrm{HW} = \frac{H}{W}, \tag{13}$$

where H is the height of the inlet and W is the width of the inlet.

The aspect ratio of the inlet has a great influence on flow conditions, such as average velocity, pressure drop, and flow morphology. The mass flow rate remains constant as the HW is varied. The flow velocity increases with the decrease of HW. For the investigation of the influence of HW on flow distribution, AR = 1 and $\alpha = 90^\circ$ is kept constant. In this paper, the value of H is 5.0 mm and remain unchanged, while the values of W are 10 mm, 15 mm and 20 mm, respectively.

As discussed in this section, a comparative study was conducted on cooling channels with different HW values. Figure 11 shows that the nonuniformity coefficient decreases as the HW value is increased. When HW is decreased to 0.25, the uniformity of flow distribution improves effectively. Therefore, a large inlet aspect ratio is beneficial to uniform flow distribution. At the same time, a small HW value is indicative of the small fluid temperature difference in each channel as shown in Figure 12.

When the HW value is decreased, the inlet areas increase and the flow velocity decreases. Figure 13 shows that the velocity in the inlet when HW = 0.25 is obviously lower than that when HW has another value. Flow distribution is uniform. The velocity distribution along the main flow direction of the inlet decides the pressure drop of each branch channel. As a result, the inlet aspect ratio should be appropriately designed to ensure that the pressure drops in each channel are similar. Heat transfer characteristics are also improved when the flow distribution in each channel is uniform.

As analyzed above, the uniform flow distribution caused by geometry structure is one of the direct reasons for the uniform temperature distribution. However, the uniform temperature distribution could in turn makes the density deviation. Figure 14 shows the influence mechanism of flow distribution in parallel channels. When the fluid is heated, the physical properties change drastically, resulting in an increase in uniform distribution. A larger heat flux to flow ratio leads to more serious heat transfer deterioration, and the cooling performance is drastically reduced. It also can be seen that a positive feedback effect exists; the uniform temperature distribution and uniform flow distribution together lead to the waste of fuel cooling capacity and heat transfer deterioration.

4. Conclusions

In this work, numerical simulation was used to study the flow distribution and heat transfer characteristics of regenerative cooling, and the effects of flow area ratio, inlet header shape, and inlet aspect ratio were analyzed. Several useful points can be obtained from this work.

(1) The nonuniformity coefficient shows great differences with the change in AR value. When the AR value is decreased, the nonuniformity coefficient decreases. Therefore, flow uniformity can be effectively improved by increasing the area of the inlet header. The maximum temperature of the wall decreases from 1334.52 K to 1220.61 K when the AR value is changed from 1 to 0.25

(2) As the inlet header shape α is decreased, the nonuniformity coefficients of each channel decrease first and then increase. The flow distribution in each channel mainly depends on the pressure drop. An appropriate reduction in inlet header shape α is beneficial to uniform flow distribution

(3) The nonuniformity coefficient decreases as the HW value is increased. The uniformity of flow distribution is effectively improved when the HW value is decreased to 0.25. The inlet aspect ratio should be properly designed to ensure that the pressure drops in each channel are similar

(4) This work shows the effects of inlet geometry parameters on flow distribution and heat transfer. In future work, the effects of fuel cracking and coking, fuel phase transition, and unsteady and heterogeneous thermal loads should be considered to improve calculation accuracy

Nomenclature

A: Area (m^2)
AR: Flow area ratio

b: Slot width (mm)
c: Spacing of channel
h: Height of channel
HW: Inlet aspect ratio
H: Height (m)
m: Mass flow rate (kg/s)
n: Number of the channels
P: Pressure (Pa)
q: Heat flux (w/m^2)
T: Temperature (K)
W: Width (m).

Greek Symbols

α: Inlet header shape
β: Nonuniformity coefficient
δ: Wall thickness (mm)
λ: Thermal conductivity (W/m·K)
u: Velocity (m/s)
ρ: Density (kg/m^3)
Ω: Scaling factor.

Subscripts

inlet: Inlet
$_{wg}$: Gas side wall
$_{wc}$: Coolant side wall
$_{\text{header}}$: Header of inlet
w: Wall.

Data Availability

The authors confirm that the data supporting the findings of this study are available within the article and its supplementary materials.

Conflicts of Interest

The authors declare that there is no conflict of interest regarding the publication of this paper.

Acknowledgments

This work was supported by the Natural Science Foundation of Hunan Province (Grant No. 2020JJ5395).

Supplementary Materials

Supplementary Figure 1: thermo-physical property variations of aviation kerosene with temperature. Supplementary Figure 2: the density fields in fluid domain with different AR values. Supplementary Table 1: viscosity of kerosene at different temperatures at $P = 3$ MPa. *(Supplementary Materials)*

References

[1] A. Paykani, C. E. Frouzakis, C. Schürch, F. Perini, and K. Boulouchos, "Computational optimization of $CH_4/H_2/CO$ blends in a spark-ignition engine using quasi-dimensional combustion model," *Fuel*, vol. 303, article 121281, 2021.

[2] H. Takahashi, M. Kodera, and K. Tani, "Flush air data sensing system for a sharp-nosed hypersonic vehicle with curved-wedge forebody," *AIAA Journal*, vol. 58, no. 11, pp. 4819–4831, 2020.

[3] L. Yin, H. P. Liu, and W. Q. Liu, "Capillary character and evaporation heat transfer in the wicks of high temperature liquid metal heat pipe," *Applied Thermal Engineering*, vol. 175, article 115284, 2020.

[4] F. Q. Zhong, X. J. Fan, G. Yu, J. Li, and C. J. Sung, "Heat transfer of aviation kerosene at supercritical conditions," *Journal of Thermophysics and Heat Transfer*, vol. 23, no. 3, pp. 543–550, 2009.

[5] Q. Zhu, Y. Zong, Y. Wenbin, W. Yang, and M. Kraft, "Understanding the particulate formation process in the engine fueled with diesel/jet A-1 blends," *Fuel*, vol. 313, article 122675, 2022.

[6] H. W. Deng, C. B. Zhang, G. Q. Xu, Z. Tao, K. Zhu, and Y. J. Wang, "Visualization experiments of a specific fuel flow through quartz-glass tubes under both sub- and supercritical conditions," *Chinese Journal of Aeronautics*, vol. 25, no. 3, pp. 372–380, 2012.

[7] C. Wang, Z. Wang, and J. Zhang, "Flow and heat transfer in a rotating cavity with de-swirl nozzles: an lES study," *International Communications in Heat and Mass Transfer*, vol. 118, article 104816, 2020.

[8] C. Yang, Z. Quan, Y. Chen, Q. Zhu, J. Wang, and X. Li, "A comprehensive investigation of the pyrolysis effect on heat transfer characteristics forn-decane in the horizon minichannel," *Energy & Fuels*, vol. 34, no. 1, pp. 199–210, 2020.

[9] Y. Chen, Z. Lei, T. Zhang et al., "Flow distribution of hydrocarbon fuel in parallel minichannels heat exchanger," *AICHE Journal*, vol. 64, no. 7, pp. 2781–2791, 2018.

[10] F. Q. Li, Z. Z. Li, K. Jing, L. Wang, X. Zhang, and G. Liu, "Thermal cracking of endothermic hydrocarbon fuel in regenerative cooling channels with different geometric structures," *Energy & Fuels*, vol. 32, no. 6, pp. 6524–6534, 2018.

[11] L. Taddeo, N. Gascoin, K. Chetehouna et al., "Experimental study of pyrolysis-combustion coupling in a regeneratively cooled combustor: system dynamics analysis," *Aerospace Science and Technology*, vol. 67, no. 1, pp. 473–483, 2017.

[12] N. Wang, Y. Jin Zhou, and H. Y. Pan, "Experimental investigation on flow patterns of RP-3 kerosene under sub-critical and supercritical pressures," *Acta Astonautica*, vol. 94, no. 2, pp. 834–842, 2014.

[13] Y. Ren, N. Mahinpey, and N. Freitag, "Kinetic model for the combustion of coke derived at different coking temperatures," *Energy & Fuels*, vol. 21, no. 1, pp. 82–87, 2007.

[14] V. R. Katta, E. G. Jones, and W. M. Roquemore, "Modeling of deposition process in liquid fuels," *Combustion Science and Technology*, vol. 139, no. 1, pp. 75–111, 1998.

[15] P. Liu, T. Zhang, L. Zhou et al., "Experimental and numerical analysis on flow characteristics and pyrolysis mechanism of hydrocarbon fuel with a novel online hybrid method," *Energy Conversion and Management*, vol. 198, article 111817, 2019.

[16] Y. Xi, X. Li, Y. Wang, B. Xu, N. Wang, and D. Zhao, "Experimental study of transition to instability in a Rijke tube with axially distributed heat source," *International Journal of Heat and Mass Transfer*, vol. 183, p. 122157, 2022.

[17] P. X. Jiang, B. Liu, C. R. Zhao, and F. Luo, "Convection heat transfer of supercritical pressure carbon dioxide in a vertical micro tube from transition to turbulent flow regime,"

International Journal of Heat and Mass Transfer, vol. 56, no. 1-2, pp. 741–749, 2013.

[18] Y. Chen, B. Liu, Z. Lei et al., "A control method for flow distribution in fuel-cooled plate based on choked flow effect," *Applied Thermal Engineering*, vol. 142, pp. 127–137, 2018.

[19] Z. Ran, G. Xu, H. Deng et al., "Characteristics of flow distribution of aviation kerosene in parallel pipes under supercritical pressure," *Journal of Aerospace Power*, vol. 27, no. 1, pp. 63–68, 2021.

[20] Y. Feng, *Research on coupling characteristics between flow and cracking of supercritical hydrocarbon*, Harbin Institure of Technoloty, 2014.

[21] T. Jing, G. He, W. Li et al., "Flow and thermal analyses of regenerative cooling in non-uniform channels for combustion chamber," *Applied Thermal Engineering*, vol. 119, p. 89, 2017.

[22] Z. Tao, X. Z. Hu, J. Q. Zhu, and H. W. Wu, "Numerical investigation of pyrolysis effects on heat transfer characteristics and flow resistance of n-decane under supercritical pressure," *Chinese Journal of Aeronautics*, vol. 31, no. 6, pp. 1249–1257, 2018.

[23] Z. Wang, Y. Wang, J. Zhang, and B. Zhang, "Overview of the key technologies of combined cycle engine precooling systems and the advanced applications of micro-channel heat transfer," *Aerospace Science and Technology*, vol. 39, no. 39, pp. 31–39, 2014.

[24] Y. Jiang, J. Qin, Y. Xu et al., "The influences of the header geometry on hydrocarbon fuel flow distribution in compact parallel channels," *Aerospace Science and Technology*, vol. 79, pp. 318–327, 2018.

[25] S. Hongyuan, *Investigation on kerosene's Regenerated Cooling of Supersonic Combustion Chamber*, National University of Defense Technology, Changsha, 2018.

[26] C. C. Wang, K. S. Yang, J. S. Tsai, and Y. Chen, "Characteristics of flow distribution in compact parallel flow heat exchangers, part I: typical inlet header," *Applied Thermal Engineering*, vol. 31, no. 16, pp. 3226–3234, 2011.